JOURNAL OF CATALYSIS 91, 116–131 (1985)

HCN Synthesis from CH_4 and NH_3 on Clean Rh[1]

D. HASENBERG AND L. D. SCHMIDT

Department of Chemical Engineering and Materials Science, University of Minnesota, Minneapolis, Minnesota 55455

Received April 13, 1984; revised September 17, 1984

A reaction chamber attached to a UHV surface analysis system is used to study kinetics of HCN synthesis on polycrystalline Rh for temperatures between 500 and 1600 K with CH_4 and NH_3 pressures between 0.05 and 10 Torr. AES is used to show that the surface is clean before reaction, and AES and TPD are used to examine surface residues after reaction. The rate of HCN production attains a maximum near a 1:1 reactant mixture, and exceeds 10^{18} molecules/cm^2 sec at high temperatures. The selectivity (fraction of NH_3 reacting to form HCN) is greater than 90% at high temperatures at a total pressure of 1 Torr. The rate of HCN production is proportional to P_{CH_4}, and N_2 formation is strongly inhibited by CH_4. Examination of rhodium foils by SEM after reaction shows that the surface is faceted into predominantly (100) planes, and grain boundaries are pitted. Reaction is shown to occur by NH_3 or its fragments reacting with surface carbon layers because approximately one monolayer of carbon is found on the reactive surface while multilayers of carbon create a totally unreactive surface. This carbon also explains why the NH_3 decomposition reaction is suppressed compared to that on clean Rh. A model in which surface carbon is a reactant which also blocks reaction sites is shown to give a quantitative fit to rates of HCN and N_2 production. The high reaction probability of CH_4 ($\sim 10^{-2}$) is surprising because of its low surface reactivity on Rh. It is argued that the surface reaction between NH_3 and CH_4 fragments is the major reaction under industrial HCN synthesis conditions and that no homogeneous processes are necessary to explain high yields of HCN. © 1985 Academic Press, Inc.

INTRODUCTION

Hydrogen cyanide is prepared industrially by reacting CH_4 with NH_3 in the Degussa process (*1, 2*)

$$CH_4 + NH_3 \rightarrow HCN + 3H_2 \qquad (1)$$

or by adding O_2 in the Andrussow process (*3–7*)

$$CH_4 + NH_3 + \tfrac{3}{2}O_2 \rightarrow HCN + 3H_2O \qquad (2)$$

The Degussa process takes place at ~1500 K with ~90% yield to HCN by reaction on platinum on tube-wall reactors, while the Andrussow reaction gives 60–70% yield at ~1400 K at atmospheric pressure in an O_2-deficient mixture over a Pt–10% Rh gauze catalyst with a contact time of much less than 1 sec.

Reaction (1) is remarkable because, while ΔG_0 is favorable at high temperature, the reaction is endothermic by 60 kcal per mole. Reactions yielding HCN are in competition with NH_3 decomposition

$$2NH_3 \rightarrow N_2 + 3H_2, \qquad (3)$$

and in O_2 with

$$4NH_3 + 3O_2 \rightarrow 2N_2 + 6H_2O, \qquad (4)$$

and

$$CH_4 + \tfrac{3}{2}O_2 \rightarrow CO + 2H_2O \qquad (5)$$

which have hearts of reaction of 11.0, −75.7, and −129.9 kcal per mole of NH_3 or CH_4. Negligible amounts of CO_2 are produced in the Andrussow process because it is run oxygen-deficient.

Figure 1 shows a plot of equilibrium constants versus $1/T$ for these and related reactions. It is seen that, while combustion reactions have very favorable equilibrium conversions at all temperatures, HCN synthesis from NH_3 and CH_4 has $K_{eq} < 1$ below

[1] This work was partially supported by NSF under Grant DMR82126729.

0021-9517/85 $3.00
Copyright © 1985 by Academic Press, Inc.
All rights of reproduction in any form reserved.

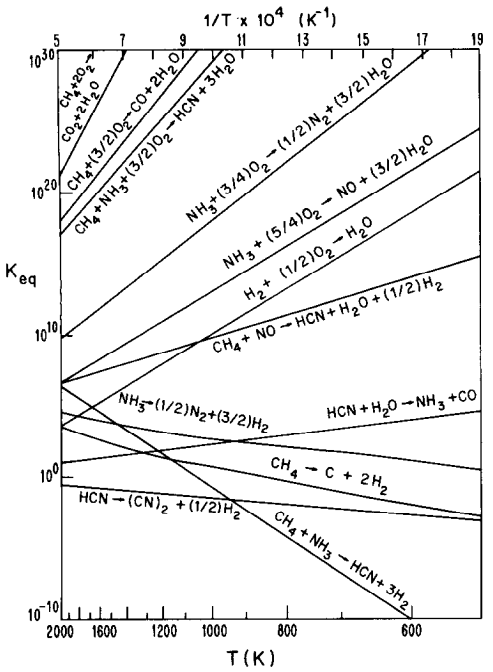

FIG. 1. Equilibrium constants for reactions of NH_3, CH_4, and O_2, calculated for standard states at 1 atm. All reactions are based on 1 mole of ammonia or 1 mole of methane. The HCN synthesis reaction is seen to be favored ($K_{eq} > 1$) only above 1000 K and to always be in competition with the thermodynamically favored ammonia and methane decomposition reactions.

1000 K. Also, NH_3 decomposition and CH_4

$$CH_4 \rightarrow C + 2H_2 \qquad (6)$$

both have more favorable equilibrium constants below 1700 K than does the HCN reaction.

NH_3 decomposition and oxidation are very fast, so that N_2 formation should compete strongly with HCN formation. Oxygen is added in the Andrussow process as a heat source. Reactions (4) or (5) provide sufficient exothermicity to maintain the catalyst temperature, and all oxygen is consumed on the first few gauze layers.

Saturated hydrocarbons and especially CH_4 are quite unreactive on noble metal surfaces (*8, 9*) (sticking probability of 2×10^{-4} at 1400 K), and this makes their reaction with NH_3 seem unlikely. At the high temperatures of the HCN converter, homogeneous reaction steps may be expected, and the surface may provide free-radical initiators for homogeneous chain reactions which ultimately produce HCN.

This study was undertaken to determine the kinetics of the surface reactions in this system on clean rhodium and platinum. Pressures between 0.1 and 10 Torr are used to eliminate homogeneous reactions because at these pressures gases are at 300 K, and wall collisions should efficiently remove the free radicals and other excited species necessary for homogeneous reaction.

This paper will be concerned with the NH_3 and CH_4 reactions on clean polycrystalline rhodium. In a later paper (*10*) we shall consider these reactions on platinum and Pt–Rh alloys, the formation of carbon from different hydrocarbons, and the effect of adding O_2 to CH_4–NH_3 mixtures.

EXPERIMENTAL

A reaction chamber was constructed using 1.5-in. stainless-steel crosses with gold-plated copper gaskets. The reaction chamber was attached through a gate valve to an ion and sublimation-pumped UHV analysis system containing AES and a mass spectrometer for surface analysis. The reaction chamber could be pumped to less than 10^{-9} Torr using the analysis system or, with the gate valve closed, to less than 10^{-8} Torr using a turbomolecular pump.

As sketched in Fig. 2, the sample, a high-purity 0.0025-cm-thick rhodium foil 2-cm long and 0.4-cm wide, was mounted on a stainless-steel plug which had four insulated molybdenum pins for resistive heating and temperature measurement using a Pt–Pt 13% Rh thermocouple spot-welded to the center of the foil. The plug could be attached to UHV feedthroughs in the reactor and in the analysis system. The plug was moved between these positions using two magnetically driven linear-rotary motion rods (Huntington) each capable of 12-

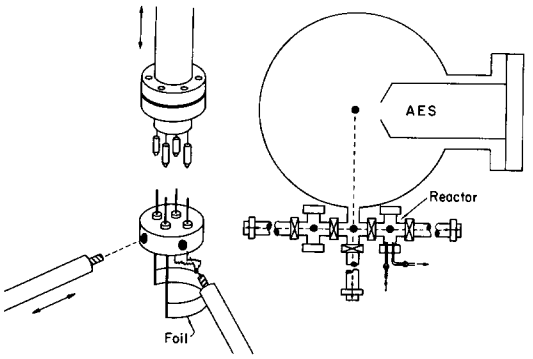

FIG. 2. Schematic diagram of system to transfer samples between analysis chamber and reaction chamber. The Rh foil is mounted on a plug with leads for resistive heating and temperature measurement. The sample is connected to heating leads in reactor and analysis chamber and is translated between chambers by magnetically coupled rods which screw into tapped holes in the side of the plug. The closed circles in the schematic denote electrical feedthrough sockets.

in. displacements and 360-degree rotation. For transfer between chambers, the rod was screwed into tapped holes in the plug, the feedthrough was pulled back, the sample was translated to the other rod, and then attached to the other feedthrough and the rod was unscrewed. Translation between feedthroughs required less than 1 min if pumpdown was not required. Samples could be introduced into the system without breaking vacuum through another 1.5-in. cross which served as a pressure interlock.

Rhodium foils were cleaned by heating above 1600 K in O_2 or NO at $\sim 10^{-7}$ Torr for several hours until all carbon and boron were removed as shown by AES (see Fig. 3). Temperatures are regarded as accurate to ± 50 K. The temperature was estimated to vary by less than 100 K between the ends and the center of the foil. Electron bombardment heating could also be used by replacing the thermocouple with a tungsten filament. Samples in the analysis chamber could be cooled to 80 K by cooling the feedthrough with liquid N_2.

An elaborate gas handling and purification system was constructed from stainless-steel tubing with bellows-sealed valves for introduction of CH_4, NH_3, H_2, NO, O_2, and CO into the reactor or the analysis chamber. Pressures between 10^{-2} and 10 Torr in the reactor were measured with a capacitance manometer, and partial pressures were measured by leaking gas from the reactor back into the analysis system at $\sim 5 \times 10^{-8}$ Torr.

Gases were purified by passing through cold, activated charcoal, and molecular sieve traps (*11*). All lines and traps were baked repeatedly until gases could be admitted without contamination of the surface. After purification, the clean Rh sample could be exposed to 10^8 L (Langmuir = 1 Torr for 100 sec) of NH_3 or CH_4 without producing more than a fraction of a mono-

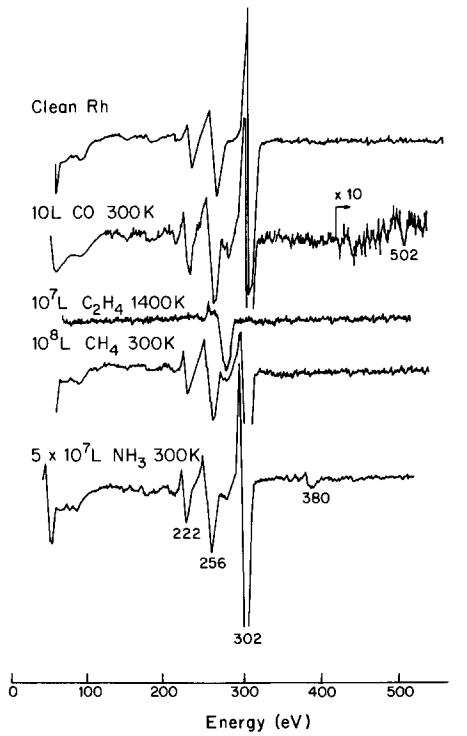

FIG. 3. AES spectra of Rh after cleaning and after exposure to gases at conditions indicated. Multilayers of carbon (270 eV) are produced by high-temperature C_2H_4 exposures, while only a monolayer or less of nitrogen (380 eV) is produced by NH_3 exposure at any temperature.

layer of carbon as indicated by AES spectra of Fig. 3.

Carbon and nitrogen coverages were calibrated against CO and NO monolayers (*12*), each assumed to be $\sim 7 \times 10^{14}$ atoms/cm^2. Exposure of 100 or 10^8 L of CO produced essentially identical AES and TPD spectra with no residual carbon contamination. AES analysis of carbon on rhodium is difficult because of overlap of the 270-eV carbon peak with several Rh peaks, although, as shown in Fig. 3, a monolayer of CO is easily detectable, and multilayer coverages can be monitored accurately.

Reaction rates were determined using the mixed reactor mass balance

$$r_i = \frac{VN_0\Delta P_i}{RT_{\text{gas}}A\tau}, \tag{7}$$

where A is the catalyst area, N_0 is Avogadro's constant, τ and V are the system residence time and volume, respectively. The residence time, determined by measuring the rate of pressure decrease from gas reservoirs of known volume, was adjusted between 0.1 and 50 sec to obtain a conversion of the limiting reactant of 2–20%.

Pressures of NH_3 and HCN are particularly troublesome to measure accurately because both gases adsorb strongly on the walls of the reactor and HCN polymerizes readily. The reactor walls and valves were heated continuously to ~370 K to reduce pumpdown time and prevent these species from freezing in valve orifices. With calibration of mass spectrometer sensitivities of all gases, use of reaction stoichiometries, and correlation with capacitance manometer measurement (an absolute total pressure calibration), we believe that measured rates are accurate to within ±20%.

Rates attained steady state within 15 sec after a temperature was established for all temperatures above 600 K at any pressures above 0.1 Torr. Apparent transients occur if NH_3 and HCN pumping characteristics are not properly accounted for. All rates shown were stable for many hours, and results were duplicated on four different rhodium foils.

RESULTS

NH_3 Decomposition

Figure 4 shows a plot of the rate of N_2 production, r_{N_2}, versus Rh foil temperature in pure NH_3 at pressures between 0.05 and 4.0 Torr. Conversions were kept below 20% so that no H_2 or N_2 product inhibition should have occurred. Surfaces were examined after reaction by AES and shown to contain only a fraction of a monolayer of nitrogen.

The rate was fit to a unimolecular Langmuir–Hinshelwood (LH) rate expression

$$r_{N_2} = \frac{k_r K_{NH_3} P_{NH_3}}{1 + K_{NH_3} P_{NH_3}} \tag{8}$$

which yielded a rate expression

$$r_{N_2} = \frac{7.5 \times 10^{18} \exp(-2130/T) P_{NH_3}}{1 + 2.5 \times 10^{-5} \exp(7000/T) P_{NH_3}} \tag{9}$$

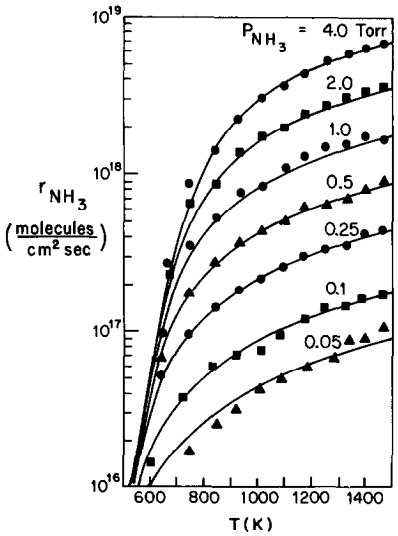

FIG. 4. Plot of r_{N_2} versus Rh foil temperature in pure NH_3 at pressures indicated. The rate goes from zeroth order to first order as temperature is increased. The solid curves are from a fit to LH kinetics for a unimolecular reaction, Eqs. (8) and (9). All data points are seen to be within ±10% of the calculated curves.

with r_{N_2} in molecules/cm^2 sec and P_{NH_3} in Torr. Solid curves were calculated using this rate expression, and it is seen that all data points are within a factor of two of the Langmuir–Hinshelwood rate expression with r_R varying by $\sim 10^3$.

Ammonia decomposition on polycrystalline Pt was studied by Loffler and Schmidt (*13*). On Rh, the reaction has been studied by Logan and Kemball (*14*) on evaporated films and by Vavere and Hansen on single crystals over a limited temperature range (*15*). The rate we measured on Rh is higher than that of Hansen and Vavere and we observed precise first-order kinetics at high temperatures while they reported half order. We believe that previous results on Rh are inaccurate or surfaces were contaminated because neither the order of the reaction nor the rates agree with those expected and observed here on a surface known to be clean.

The rate of NH_3 decomposition approaches 10^{19} molecules/cm^2 sec at 1400 K which represents a reaction probability (fraction of incident NH_3 flux decomposing to N_2 and H_2) of 0.002. Thus, NH_3 decomposition is sufficiently fast that HCN should only be found in significant amounts if its rate is greater than that of r_{N_2} in pure NH_3 or if the presence of CH_4 decreases r_{N_2}.

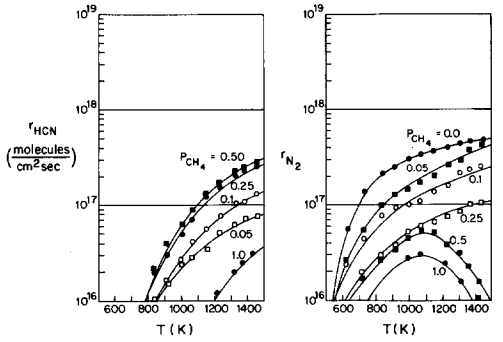

FIG. 5. Plots of r_{HCN} and r_{N_2} versus Rh foil temperature for P_{NH_3} = 0.25 Torr at CH_4 pressures indicated. Rates are obtained using Eq. (6) with conversions less than 20%. Solid curves are drawn through sets of data at a fixed gas composition.

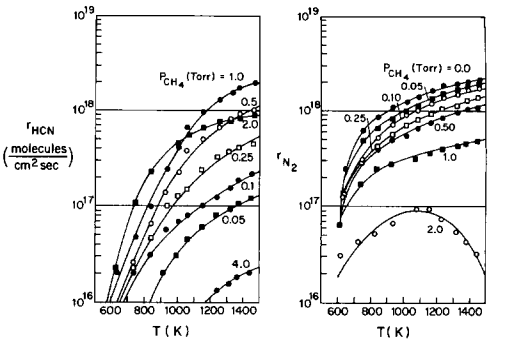

FIG. 6. Plots of r_{HCN} and r_{N_2} versus Rh foil temperatures for P_{NH_3} = 1.0 Torr at methane pressures indicated.

HCN Synthesis

Figures 5 and 6 show typical plots of r_{HCN} and r_{N_2} versus Rh foil temperature for fixed P_{NH_3} = 0.25 and 1.0 Torr, respectively. Values of P_{CH_4} are indicated in the figures. Data were obtained by establishing fixed pressures and varying the foil temperature. Steady states were established within 15 sec, and rates at a given temperature were always identical when approached from lower and higher temperatures. The minimum detectable rate, limited by the lowest detectable partial pressure changes, was approximately 5×10^{15} molecules/cm^2 sec. In excess CH_4, the rates decrease approximately as $P_{CH_4}^{-4}$, and these rates are therefore very sensitive to slight pressure changes.

Comparable sets of rates versus temperature were obtained at P_{NH_3} = 0.1, 0.5, 2.0, and 4.0 Torr, with all curves having the same general shape as those shown in Figs. 5 and 6: r_{HCN} first increases with P_{CH_4} and then decreases while r_{N_2} decreases monotonically with P_{CH_4}.

Figure 7 shows plots of r_{HCN} and r_{N_2} versus P_{CH_4}, while Fig. 8 shows plots of r_{HCN} and r_{N_2} versus P_{NH_3} for a Rh temperature of 1450 K. These curves were obtained from rate versus temperature curves similar to Figs. 5 and 6 by extrapolating between measured rates near this temperature.

It is seen from Fig. 7 that r_{HCN} is proportional to P_{CH_4} in excess NH_3 while r_{HCN} is

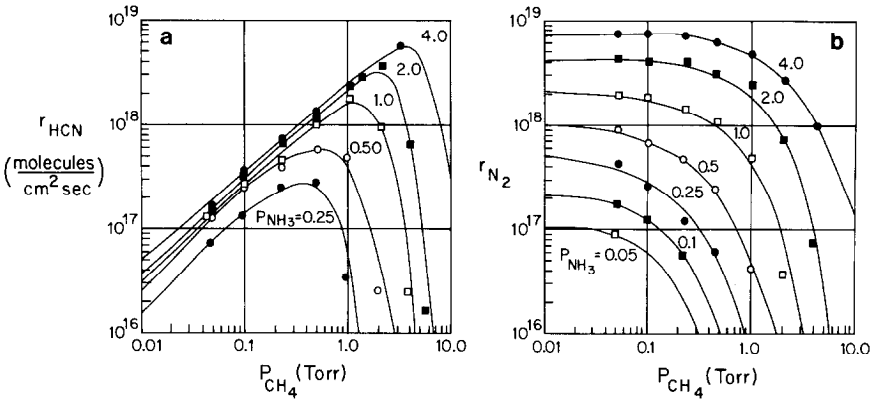

FIG. 7. Plots of r_{HCN} and r_{N_2} versus P_{CH_4} at 1450 K for NH_3 pressures indicated. The r_{HCN} increases with P_{CH_4} and then decreases steeply, while r_{N_2} is initially constant and then decreases steeply with P_{CH_4}.

strongly inhibited by CH_4 in excess CH_4. Figure 8 shows that r_{HCN} is proportional to P_{NH_3} in excess NH_3 and to a higher power of P_{NH_3} in excess CH_4.

The curve in Fig. 8b with $P_{CH_4} = 0$ is identical to the data from Fig. 4 at 1450 K as expected. These results show that CH_4 strongly inhibits NH_3 decomposition to N_2 even at 1450 K. The order of r_{N_2} increases from first order to approximately third order when CH_4 is present, and the rate decreases by several orders of magnitude. Figure 7b shows that, for large P_{CH_4}, r_{N_2} is inhibited as approximately fourth order in P_{CH_4}.

Surface Coverages

Figure 9 shows AES spectra of the Rh foil after exposure to CH_4 and NH_3 at 1 Torr at 300 and at 1400 K. All surfaces were cooled to 300 K before gases were pumped out. Rapid attainment of steady-state reaction rates suggests that coverages attained steady state quickly, and we find that AES spectra are nominally independent of the time of exposure to gases at high pressure.

Heating in C_2H_4 always produced a carbon layer so thick that no Rh peaks are visible (>30 Å). At 300 K, 10^8 L of CH_4 produces approximately one monolayer of car-

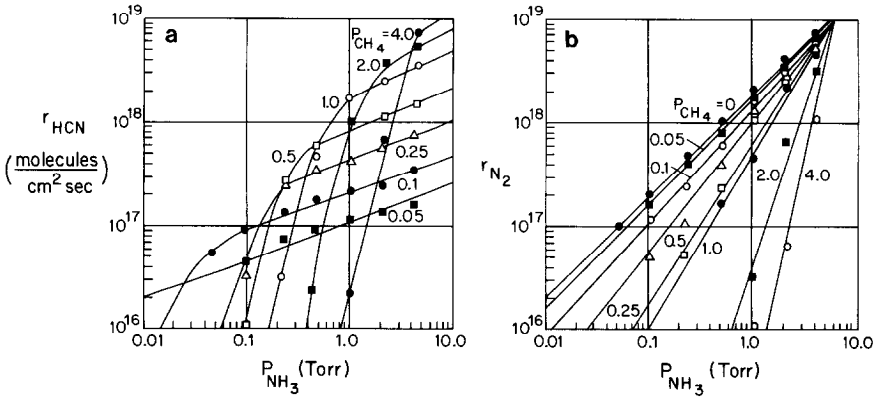

FIG. 8. Plots of r_{HCN} and r_{N_2} versus P_{NH_3} at 1450 K for methane pressures indicated.

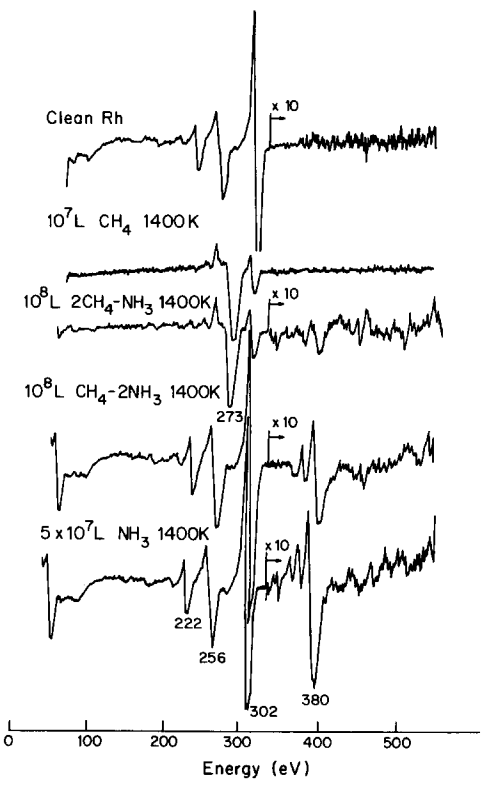

FIG. 9. AES spectra of Rh foil after heating in methane and ammonia at exposures indicated at 1400 K. The reactive surface (1:2 CH_4:NH_3) contains less than one monolayer of carbon or nitrogen while the unreactive surface (2:1 CH_4:NH_3) contains a multilayer of carbon.

bon (comparable to the carbon peak from CO saturation). Heating to 1400 K in CH_4 produces a large carbon signal, but the major Rh peak is still evident. We estimate this carbon thickness to be ~15 Å (*16*). Other experiments in which the carbon coverage was determined by measuring CH_4 pumping in a batch configuration confirm that multilayer coverages of carbon form very slowly by CH_4 decomposition.

While nitrogen could be easily detected following high exposures to NH_3, its coverage was never more than one monolayer. Heating this surface above 1000 K reduced the nitrogen signal to much less than a monolayer, but the last traces of nitrogen could only be removed by extensive heating above 1600 K. We believe that this stable nitrogen is a bulk nitride which appears to have a negligible effect on reaction kinetics.

Low coverage exposure (<1000 L) to NH_3 produced much less than a monolayer of nitrogen (calibrated against low-pressure saturation of NO) at 300 K, while large exposures to (>10^7 L) NH_3 produced ~1 monolayer of nitrogen. Negligible carbon was deposited on the surface by these treatments. Exposure to CH_4–NH_3 mixtures produced nominally one monolayer of nitrogen and carbon in excess NH_3. Note that the amount of nitrogen produced by these conditions is considerably less than that produced by exposure to NH_3 alone.

In excess CH_4 (a 2:1 CH_4:NH_3 mixture), a multilayer of carbon is formed with an AES spectrum indistinguishable from that obtained after heating in pure CH_4.

TPD spectra of adsorbed methane, ammonia, and coadsorbed CH_4–NH_3 mixtures are shown in Fig. 10. Mass 27(HCN), 28(N_2), and 2(H_2) spectra are shown with coverages calibrated against a CO mass-28 monolayer and a H_2 mass-2 monolayer obtained by saturation in H_2 at 100 L (*17*).

Methane does not adsorb appreciably on Rh at 300 K in that both AES and TPD show essentially clean surfaces after exposure to 10^8 L CH_4. At elevated temperatures, CH_4 forms a carbon multilayer, and TPD spectra show no desorption of CH_4 and only a trace amount of H_2. Methane adsorption at high temperature is therefore dissociative and irreversible. The AES line shape shows a graphitic residue as does C_2H_4 (Figs. 3 and 9) (*18*).

Ammonia also does not desorb as NH_3 from Rh following a 5×10^7 L NH_3 exposure at 300 K. High exposure to ammonia produces dissociation and the resulting TPD spectrum shows approximately a N_2 monolayer with less than 0.01 monolayer of H_2. Similar results were noted by Mummey and Schmidt for 10^9 L exposures of NH_3 on Pt (*11*).

Coadsorption of methane and ammonia at the HCN synthesis temperature of 1400 K causes a marked change in the mass-28

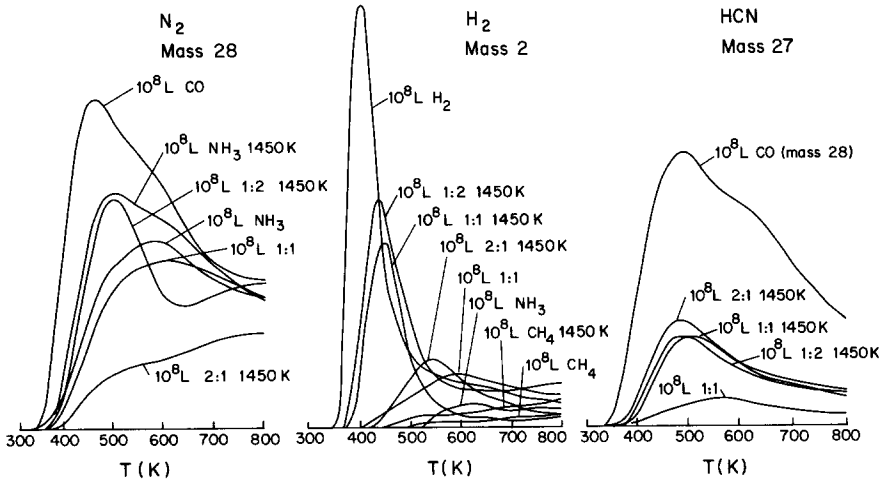

FIG. 10. TPD spectra of N_2, H_2, and HCN following reaction at conditions indicated. High exposures to NH_3 to produce approximately a CO monolayer density of N_2 except in excess methane. Very little H_2 or HCN are desorbed from the reactive surface. Note that all experiments involve cooling to 300 K before pumpdown for TPD. Heating rates were approximately 50 K/sec. Ratios of gases are indicated as methane : ammonia. All spectra are on a surface at 300 K unless otherwise indicated.

TPD spectra. In excess NH_3, TPD shows that the high-temperature state of N_2 is depleted, while the low-temperature state remains unaffected. As the CH_4–NH_3 ratio is increased, the coverage of nitrogen is reduced proportionally and AES of these surfaces shows carbon multilayer formation.

The coverage of H_2 is small after high exposures to methane or ammonia. We attribute the H_2 desorption peak ($\sim\frac{1}{3}$ monolayer) after a 10^8 L exposure to a mixture of methane in excess ammonia to gases adsorbed upon cooling and pumpdown.

The mass-27 (HCN) signal is always less than $\frac{1}{3}$ of a CO monolayer. HCN desorbs readily after it is formed at high temperatures.

Thus, TPD of the Rh surface following HCN synthesis shows that (1) no carbon-containing residues desorb under any conditions, (2) little hydrogen is present, (3) in excess CH_4 carbon effectively blocks adsorption of other species, and (4) a significant amount ($\sim\frac{1}{3}$ monolayer) of HCN desorbs from the active surface. It should of course be noted that various species can adsorb upon cooling in gases. However, the *absence* of species strongly suggests their absence under reaction conditions. These results are in good agreement with AES and kinetic results and give further support to the importance of surface carbon in the process.

Surface Structure

Rhodium lost its mirror appearance after a few hours of heating in reacting gases at high pressures. Figure 11 shows SEM micrographs of a Rh foil after reaction for many hours. The region shown was near the center, but all regions appeared essentially identical except that faceting was less pronounced near the cooler ends of the foil.

It is seen that grain boundaries are clearly outlined by pitting. The average grain size is ~ 15 μm, and pit diameters are ~ 5000 Å. Pits occur in regular arrays along most grain boundaries, although some boundaries have few or no pits and some are opened into grooves. The pitting process is evidently specific to particular grain crystallography.

Most grain faces are faceted. These facets are generally of one type and have a specific periodicity (~ 1.25 μm between

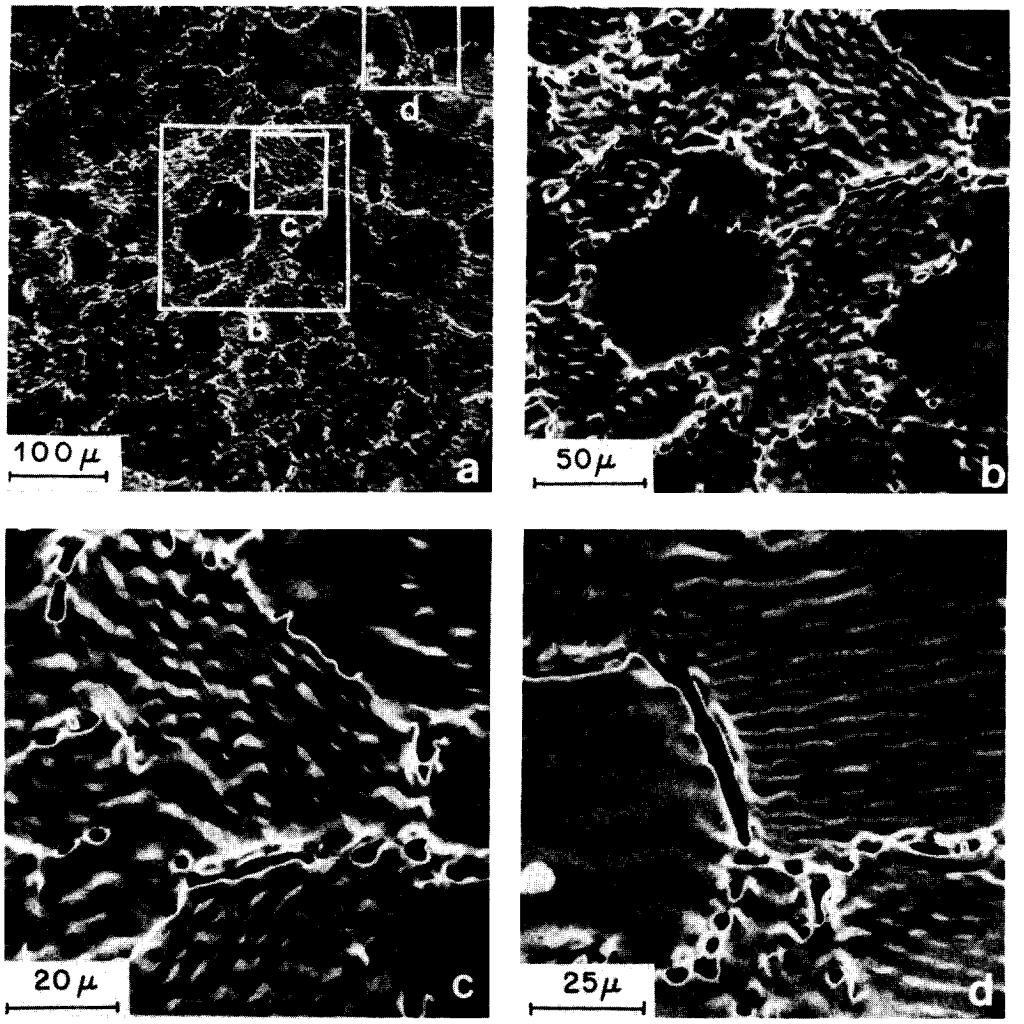

FIG. 11. SEM micrographs of a Rh foil after use in the $CH_4 + NH_3$ reaction. Grain boundaries are extensively pitted and many grain faces are faceted to form predominantly (100) facets.

facets) on each grain. A few grains remain smooth. Examination of facets on many grains shows that most facets are approximately 90 degrees from each other. From this we infer that the faceted surface consists predominantly of (100) crystal planes. Faceting is presumably associated with a reduced surface free energy of certain crystallographic orientations (evidently (100)). For example, if carbon formed preferentially on (100), this could stabilize this plane sufficiently to produce predominantly this orientation.

Catalytic etching of platinum and rhodium has been studied extensively in this and other laboratories (*19*). Etching is usually most rapid in atmospheres containing O_2 because both faceting and pitting can occur by formation of volatile oxides. In the present situation, surface diffusion is the only mechanism of etching because no O_2 is present. The reaction is also strongly endothermic so that hot spots from reaction heat cannot accelerate etching.

Pit formation appears to be greater on rhodium than on platinum or other noble metals. This is probably associated with some type of species at grain boundaries

(e.g., carbon or nitrogen) which promotes this mode of attack.

DISCUSSION

To summarize these results, rates are found to attain unique and reproducible steady states with the following dependences on P_{CH_4} and P_{NH_3}:

$$r_{HCN} \propto P_{CH_4} P_{NH_3}^{1/2} \tag{10}$$

and

$$r_{N_2} \propto P_{NH_3} \tag{11}$$

in excess NH_3 and

$$r_{HCN} \propto P_{CH_4}^{-4} P_{NH_3}^{\sim +3} \tag{12}$$

and

$$r_{N_2} \propto P_{CH_4}^{-4} P_{NH_3}^{\sim 3} \tag{13}$$

in excess CH_4. These dependences come from asymptotic slopes of Figs. 7 and 8 at 1450 K. Essentially identical pressure plots were obtained at 1100 K, and we conclude that these pressure dependences are valid for any temperature above 900 K.

AES and TPD of surfaces giving these kinetics showed that $\theta_C \leq 1$ and $\theta_N \leq 1$ in excess ammonia and $\theta_C \geq 1$ and $\theta_N \ll 1$ in excess CH_4. It is clear from the correlation of kinetics and surface characterization that the reactive surface (excess NH_3) contains less than one monolayer of either carbon or nitrogen and that the unreactive surface (excess CH_4) contains a multilayer of carbon.

In the following sections we shall consider possible surface and kinetic models which are consistent with these results.

Reaction Rates

We assume first that the rates of HCN formation can be written as

$$r_{HCN} = k\theta_C\theta_N, \tag{14}$$

implying that a carbon-containing species must combine with a nitrogen-containing species to form the CN bond which leads to HCN. These species should be partially or totally dehydrogenated and be written as CH_{x_s} and NH_{y_s}, although several partially dehydrogenated species may exist.

The corresponding expression for N_2 formation should be

$$r_{N_2} = k\theta_N \text{ or } k\theta_N^2 \tag{15}$$

in that this rate could involve unimolecular or bimolecular limiting steps.

Since the temperatures of interest are above 1000 K, very few species can exist on the surface at reaction temperatures. We shall use Langmuir (one-state) models of the coverages and processes in discussing results. While there should be crystallographic and binding state averaging on polycrystalline Rh, these effects almost always produce averages which are insensitive to details of the adsorption states and processes (i.e., averages are approximately linear). It is easy to estimate coverages assuming a Langmuir isotherm, $\theta_i = k_i P_i/(1 + k_i P_i)$ with the equilibrium constant given by

$$k_i = k_0 \exp(\Delta H/RT) = \frac{S_0}{k_{d0}(2\pi MRT_g)^{0.5}} \exp\left\{\frac{\Delta H_i}{RT}\right\}. \tag{16}$$

If the initial sticking coefficient S_0 is 1 and the desorption preexponential factor k_{d0} is 10^{13} sec^{-1}, the steady-state coverage is less than 10^{-2} monolayers at 1000 K for any species whose heat of adsorption is less than 25 kcal/mole. Measured heats of adsorption of gaseous species on Pt are $E_{NH_3} = 17$ kcal/mole, $E_{N_2} \sim 25$ kcal/mole, $E_{H_2} = 25$ kcal/mole, and $E_{CH_4} \leq 10$ kcal/mole. In clean surface experiments on Pt, nitrogen atoms desorb as N_2 with this heat of adsorption although N_2 cannot be adsorbed (*20, 21*), and NH_3 desorbs with little decomposition at low pressures (*22*). Bridge and Lambert (*23, 24*) report that HCN adsorbs dissociatively on Pt(110), and Netzer *et al.* (*25, 26*) report that CN is the stable species following cyanogen exposures to Pt(100). On rhodium, CH_4 has not been observed to chemisorb (*8, 9*), H_2 adsorbs dissociatively (*17*), and CH_3NC adsorbs nondissociatively

at 120 K, but decomposes to hydrogen, nitrogen, and HCN above room temperature (*27, 28*). While properties of these species could deviate from those observed in clean-surface experiments at low pressure and temperature, these estimates should yield accurate upper bounds on coverages.

Many fragments which do not exist as stable gas molecules such as CH_x, NH_y, and CN could exist on the surface at high concentrations. An upper bound on the coverage of such species can be obtained by estimating their adsorption lifetimes τ_i from the expression

$$\tau_i \simeq k_{d_i}^{-1} = k_{d0_i}^{-1} \exp\left\{\frac{-\Delta H}{RT}\right\} \theta, \qquad (17)$$

where the desorption activation energy is assumed to be equal to the heat of adsorption. For $k_{d0} = 10^{13}$ sec^{-1}, we obtain adsorption lifetimes of 10^{-7} to 10^{-8} sec if $E_d = 25$ kcal/mole and 10^{-3} to 10^{-5} sec if $E_d = 50$ kcal/mole. Thus, any species with a heat of adsorption (to any product) less than these values should have these lifetimes for unimolecular desorption.

We therefore assume that very few species can have coverages and adsorption lifetimes required to attain sufficient coverage to block surface sites. The only likely candidates are CH_x and NH_y. Decomposition of adsorbed ammonia, $NH_3 \rightarrow NH_2 + H \rightarrow NH + H \rightarrow N + H$, appears to be quite rapid, and, while each of these species has been identified on Pt at lower temperatures and pressures, we do not believe that any of these species is sufficiently stable to prevent complete dissociation and desorption as N_2 and H_2 (*29*). Methane decomposition, $CH_4 \rightarrow CH_3 + H \rightarrow CH_2 + H \rightarrow CH + H \rightarrow C + H$, does not yield gaseous paths for carbon desorption except as CH_4, HCN, and C_2N_2. We believe that carbon diffusion in Rh is rapid at high temperatures so that the carbon concentration in the bulk metal reaches steady state rapidly (*30*). Also, from attempts to clean carbon from Rh, it is known to be stable to the melting point in the absence of oxidizing gases.

Thus, one could write the rate steps in these reactions as

$$\begin{aligned} CH_{4g} &\rightarrow CH_{x_s} \\ NH_{3g} &\rightarrow NH_{y_s} \\ CH_x + NH_y &\rightarrow HCN + (x + y - 1)/2\ H_2 \\ 2NH_y &\rightarrow N_2 + yH_2. \end{aligned} \qquad (18)$$

In this sequence all species on the right-hand sides of the equations, except CH_x and NH_y, are assumed to be formed irreversibly and desorb quickly.

It is straightforward to write surface species mass balance equations for assumed x and y and to solve these equations to find r_{HCN} (P_{NH_3}, P_{CH_4}) and r_{N_2} (P_{NH_3}, P_{CH_4}). However, the expressions for the θ's are invariably polynomials with a large number of unknown coefficients. Such expressions can only be fit numerically to experimental data.

Therefore, we shall examine several simplified models of the processes in order to obtain expressions from which the pressure and temperature dependences can easily be extracted. If we assume that CH_4 and NH_3 adsorb reversibly to some form of carbon and nitrogen species θ_C and θ_N, it is simple to write expressions for carbon and nitrogen. (We shall write these coverages to designate unspecified partially hydrogenated species containing carbon and nitrogen atoms.) Mass balances yield

$$\frac{d\theta_C}{dt} = ka_{CH_4}P_{CH_4}(1 - \theta_C - \theta_N) - kd\theta_C = 0 \qquad (19)$$

and

$$\frac{d\theta_N}{dt} = ka_{NH_3}P_{NH_3}(1 - \theta_C - \theta_N)^2 - kd\theta_N^2 = 0. \qquad (20)$$

In these expressions, we have arbitrarily assumed competitive adsorption and that NH_3 adsorbs in two sites. The latter is reasonable (but certainly not required) for a

dissociated species which requires two sites for fragments. The Langmuir isotherms now become

$$\theta_C = \frac{K_{CH_4}P_{CH_4}}{1 + K_{NH_3}^{1/2}P_{NH_3}^{1/2} + K_{CH_4}P_{CH_4}} \quad (21)$$

and

$$\theta_N = \frac{K_{NH_3}^{1/2}P_{NH_3}^{1/2}}{1 + K_{NH_3}^{1/2}P_{NH_3}^{1/2} + K_{CH_4}P_{CH_4}}. \quad (22)$$

The products HCN and N_2 are formed through bimolecular processes involving carbon and nitrogen, Eqs. (14) and (15), then the rates become

$$r_{HCN} = \frac{k_{HCN}K_{CH_4}K_{NH_3}^{1/2}P_{CH_4}P_{NH_3}^{1/2}}{(1 + K_{NH_3}^{1/2}P_{NH_3}^{1/2} + K_{CH_4}P_{CH_4})^2} \quad (23)$$

and

$$r_{N_2} = \frac{k_{N_2}K_{NH_3}P_{NH_3}}{(1 + K_{NH_3}^{1/2}P_{NH_3}^{1/2} + K_{CH_4}P_{CH_4})^2}. \quad (24)$$

These expressions give qualitatively correct fits to experimental data. The HCN rate is first order in P_{CH_4} at low P_{CH_4} and inhibited as $P_{CH_4}^{-1}$ at high P_{CH_4}. The N_2 rate goes from first order in P_{NH_3} at low P_{CH_4} and is inhibited as $P_{CH_4}^{-2}$ in high P_{CH_4}. The order of the reactions, M, in P_{CH_4} and P_{NH_3} predicted by these very simple models are therefore $-1 < M\ CH_4 < +1$ and $-\frac{1}{2} < M\ NH_3 < +\frac{1}{2}$ for HCN synthesis and $0 < M\ NH_3 < +1$ and $-2 < M\ CH_4 < 0$ for NH_3 decomposition.

Site-Blocking Model

While the model just considered yields correct signs of CH_4 and NH_3 promotion and inhibition of both reactions, it does not yield the proper CH_4 inhibition in excess CH_4, $r \sim P_{CH_4}^{-4}$. We shall consider next a simple variation on this model which yields, with simplification, an expression which gives a quantitative fit to all kinetic data. We note again that more complete expressions always give polynomials with many rate coefficients from which the uniqueness of any particular assumption is difficult to assess.

We assume that reactions occur by NH_3 reacting with a carbon-containing Rh surface and that rates are given by expressions of the form

$$r_{HCN} = k_{HCN}\theta_C(1 - \theta_C)^n P_{NH_3} \quad (25)$$

and

$$r_{N_2} = k_{N_2}(1 - \theta_C)^n P_{NH_3}. \quad (26)$$

This dependence on $(1 - \theta_C)^n$ would arise if reaction required n vacant sites. This could be caused by a steric requirement or electronic alterations of the surface structure by adsorbed carbon which inhibits both reactions.

If the fraction of vacant sites is small, then $1 \ll K_{NH_3}^{1/2}P_{NH_3}^{1/2}$, K_CP_C, and θ_C and $(1 - \theta_C)$ become

$$\theta_C = \frac{KP_{CH_4}/P_{NH_3}^{1/2}}{1 + KP_{CH_4}/P_{NH_3}^{1/2}} \quad (27)$$

and

$$1 - \theta_C = \frac{1}{1 + KP_{CH_4}/P_{NH_3}^{1/2}}, \quad (28)$$

where $K = K_{CH_4}/K_{NH_3}^{1/2}$. Inserting these expressions into Eqs. (25) and (26) we obtain

$$r_{HCN} = \frac{k_{HCN}KP_{CH_4}P_{NH_3}^{1/2}}{(1 + KP_{CH_4}/P_{NH_3}^{1/2})^{n+1}} \quad (29)$$

and

$$r_{N_2} = \frac{k_{N_2}P_{NH_3}}{(1 + KP_{CH_4}/P_{NH_3}^{1/2})^n}, \quad (30)$$

where $K = K_{CH_4}/K_{NH_3}^{1/2}$.

Thus we obtain the following dependences on P_{CH_4} and P_{NH_3}

$$r_{HCN} \propto P_{CH_4}P_{NH_3}^{1/2}$$

and

$$r_{N_2} \propto P_{NH_3}, \quad K_{NH_3}^{1/2}P_{NH_3}^{1/2} > K_{CH_4}P_{CH_4} \quad (31)$$

and

$$r_{HCN} \propto P_{CH_4}^{-n} P_{NH_3}^{(n+2)/2}$$

and

$$r_{N_2} \propto P_{CH_4}^{-n} P_{NH_3}^{(n+2)/2},$$

$$K_{NH_3}^{1/2} P_{NH_3}^{1/2} > K_{CH_4} P_{CH_4}. \quad (32)$$

If $n = 4$, these become

$$r_{HCN} \propto P_{CH_4} P_{NH_3}^{1/2}$$

and

$$r_{N_2} \propto P_{NH_3}, \quad (33)$$

when $K_{CH_4} P_{CH_4} < K_{NH_3}^{1/2} P_{NH_3}^{1/2}$ and

$$r_{HCN} \propto P_{CH_4}^{-4} P_{NH_3}^{3}$$

and

$$r_{N_2} \propto P_{CH_4}^{-4} P_{NH_3}^{3}, \quad (34)$$

when $K_{CH_4} P_{CH_4} > K_{NH_3}^{1/2} P_{NH_3}^{1/2}$.

Figures 12 and 13 show plots of r_{HCN} and r_{N_2} versus P_{CH_4} and P_{NH_3} obtained from Eqs. (29) and (30) with $n = 4$. These were obtained from best fits of data from Figs. 7 and 8 at 1450 K. Note that these equations contain only three rate coefficients k_{HCN}, k_{N_2}, and K, and the number of vacant sites n taken here as four.

The fits to experimental data at 1450 K are essentially quantitative with all points within a factor of three of the calculated curves. Some experimental points may in fact contain systematic errors as large as this because of possible errors in pressure or temperature measurement.

Corresponding plots of r_{HCN} and r_{N_2} versus P_{CH_4} and P_{NH_3} from data at 1100 K were also fit using Eqs. (29) and (30). From fits at 1450 and 1100 K, the temperature dependence of rate coefficients was fit to Arrhenius dependences. These yielded the rate expressions

$$r_{HCN} = \frac{4.5 \times 10^{18} \exp(-1000/T) P_{CH_4} P_{NH_3}^{1/2}}{(1 + 0.0367 \exp(2500/T) P_{CH_4}/P_{NH_3}^{1/2})^5} \quad (35)$$

and

$$r_{N_2} = \frac{7.5 \times 10^{18} \exp(-2130/T) P_{NH_3}}{(1 + 0.0367 \exp(2500/T) P_{CH_4}/P_{NH_3}^{1/2})^4}. \quad (36)$$

This model is by no means unique, but we believe that all assumptions are plausible and, in most cases, the most plausible of alternative reaction steps. Only $(1 - \theta_C)^n$ or $\exp(-\alpha\theta_C)$ factors can yield the strong CH_4 inhibition which we observed. The assumption of NH_3 adsorbing dissociatively in two sites was postulated to explain the $P_{NH_3}^{1/2}$ de-

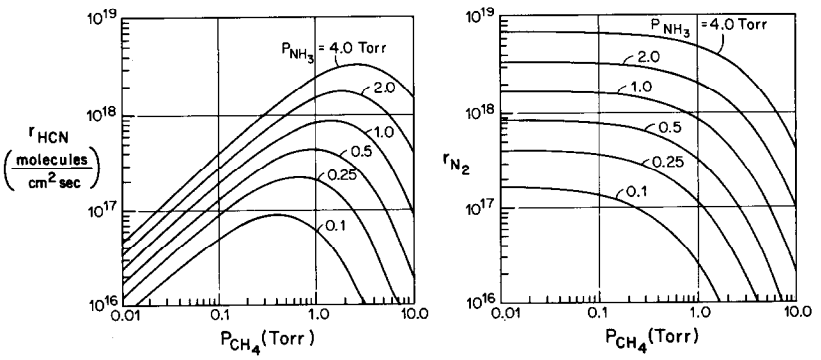

FIG. 12. Plots of r_{HCN} and r_{N_2} versus P_{CH_4} at 1450 K using the LH model of Eqs. (35) and (36). Rates are seen to be within a factor of two of all data points in Fig. 7.

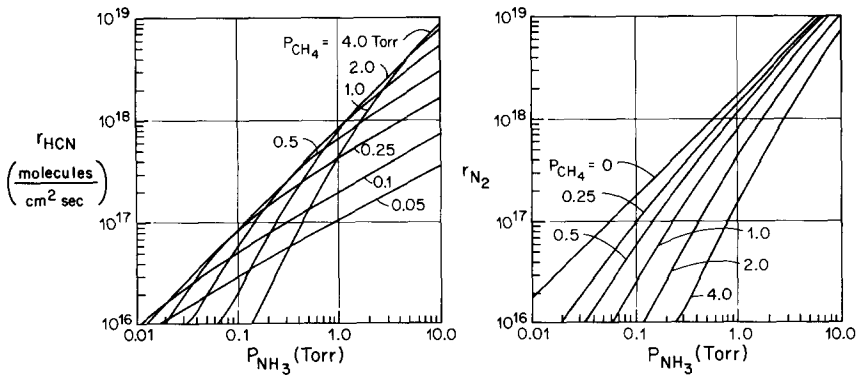

FIG. 13. Plots of r_{HCN} and r_{N_2} versus P_{NH_3} using the LH model of Eqs. (35) and (36). Rates agree well with data of Fig. 8.

pendence of r_{HCN}. The single site assumption for CH_4 was used to obtain a P_{CH_4} dependence as observed experimentally. The number of vacant sites (n) was chosen to be four because rates are inhibited approximately as $P_{CH_4}^{-4}$ which yields $n = 4$ in Eqs. (29) and (30). In fact, choice of $n = 5$ or 6 yields an equally good fit to rates versus pressures. Probably the most questionable assumption in deriving the rates is that of making both rates proportional to P_{NH_3} in Eqs. (25) and (26). One interpretation of this is that rates are NH_3 adsorption limited, but this assumption is inconsistent with the adsorption equilibrium isotherm for ammonia. We also formulated isotherms for ammonia and methane without including H_2 dependences. As noted previously, rates did not depend strongly on hydrogen, and the isotherms of Eqs. (21) and (22) should be regarded mainly as convenient representations of the adsorption steps of methane and ammonia.

Reactive Complexes

The model just described assumes basically that ammonia reacts with surface carbon to form HCN or with itself to form N_2. The strong inhibition of both reactions by excess methane and the good fits of rate expressions developed using this model are evidence that these overall processes are qualitatively correct.

The exact nature of the CH_x and NH_y fragments is of course unknown. We believe that dehydrogenation is very fast above 1000 K so that carbon is totally dehydrogenated ($x = 0$). If ammonia reacts with this carbon very quickly, it may not be totally dehydrogenated ($y > 0$), and it is plausible that nitrogen atoms on the surface will react only to N_2.

Cyanide groups are well known ligands in organometallic chemistry (*31*), and CN can bond to transition metal atoms (including Rh) as NC–, CN–, –CN–, and as π side-bonded complexes. Addition of H to any of these adsorbate–metal bonds could produce HCN.

However, we see very little cyanogen (C_2N_2) or methylamine (CH_3NH_2) or acetonitrile (CH_3CN), formed in this reaction. These would be expected products if CN or CH_3 complexes existed on the surface. Thus, we speculate that a reactive complex involving C and NH_3 gives the best agreement with kinetic and selectivity data.

In postulating intermediates it should be remembered that most adsorbate lifetimes must be very short and steady-state coverages very low at high temperatures. Thus, H atoms and N atoms should have very low concentrations so that bimolecular reaction steps such as H + CN → HCN or N + CH → HCN would be improbable. Since carbon has a measurable coverage, the process NH + C → HCN seems to be the most reasonable.

The high reactivity of methane with Rh is surprising in view of its total unreactivity at low temperatures (*8, 9, 33–35*). Stewart and Ehrlich estimated the sticking coefficient of CH_4 on clean Rh and found it to be activated with an activation energy of 7 kcal/mole. For a temperature of 1400 K s_{CH_4} should be 3×10^{-4}. They observed a large dependence of s on gas temperature and, since the CH_4 temperature in our experiments is ~300 K, their results would predict a very small sticking coefficient for CH_4 in our experiments. We observe a reaction probability of methane to HCN approaching 0.01. Methane dissociation must occur more readily on a carbon covered surface than on a clean metal surface. Energy accommodation, a necessary step in the adsorption process, should be more efficient on a surface of low atomic number. There has been discussion covering vibrational activation of CH_4 for adsorption; these experiments suggest that the nature of the surface also plays an important role in sticking.

Remarkably simple rate expressions, Eqs. (35) and (36), fit all rate data over wide ranges of temperature, pressure, and gas composition. While these rate expressions are clearly not the only ones that could be postulated, the mechanism they imply is quite plausible. This mechanism is a rather simple Langmuir–Hinshelwood path and it seems to be applicable over the entire range of the experiments. Note also that the model is a strict monolayer model which requires that the rates approach zero as $\theta_C \rightarrow 1$. One could easily postulate more complex models, but more complexity is unnecessary because this model gives a satisfactory fit to all data.

In future papers we shall examine this reaction on Pt and Pt–Rh alloys and shall consider the effects of adding O_2. However, from results shown here it is clear that the Degussa reaction provides a favorable path to HCN synthesis even in the absence of oxygen.

SUMMARY

This reaction seems highly improbable: unfavorable equilibrium composition, unfavorable competition with NH_3 decomposition to N_2 and CH_4 decomposition to graphite, possibility of HCN fragmentation on a surface at 1500 K. However, CH_4 and NH_3 react with greater than 90% probability to form HCN on Rh or Pt. The reaction requires several "windows" in that CH_4 and NH_3 must dissociate but neither N_2 nor graphite can form to any appreciable extent.

This reaction is definitely metal-catalyzed because both rates go to zero for multilayer carbon coverages. Carbon is both a reactant and a poison because the reactive surface needs both free metal sites for NH_3 adsorption and carbon-filled sites to block NH_3 decomposition to N_2. Most reactions in which carbon is an intermediate (for example, CO hydrogenation) probably exhibit similar promotion and poisoning by carbon (*32*).

REFERENCES

1. Koberstein, E., *Ind. Eng. Chem. Process Des. Dev.* **12,** 444 (1973).
2. Endter, F., *Platinum Met. Rev.* **6,** 9 (1962).
3. Satterfield, C. N., "Heterogeneous Catalysts in Practice," p. 221. McGraw–Hill, New York, 1980.
4. Pan, B. Y. K., and Roth, R. G., *J. Catal.* **21,** 27 (1971).
5. Pan, B. Y. K., and Roth, R. G., *Ind. Eng. Chem. Process Des. Dev.* **7,** 53 (1968).
6. Pan, B. Y. K., *Ind. Eng. Chem. Process Des. Dev.* **8,** 262 (1969).
7. Pirie, J. M., *Platinum Met. Rev.* **2,** 7 (1958).
8. Stewart, C. N., and Ehrlich, G., *J. Chem. Phys.* **62,** 4672 (1975).
9. Brass, S. G., Reed, D. A., and Ehrlich, G., *J. Chem. Phys.* **70,** 5244 (1979).
10. Hasenberg, D., and Schmidt, L. D., in preparation.
11. Mummey, M. J., and Schmidt, L. D., *Surf. Sci.* **91,** 301 (1980).
12. Gorte, R. J., and Schmidt, L. D., *Surf. Sci.* **111,** 260 (1981).
13. Loffler, D. G., and Schmidt, L. D., *J. Catal.* **41,** 440 (1976).

14. Logan, S. R., and Kemball, C., *Faraday Soc. Trans.* **56,** 144 (1960).
15. Vavere, A., and Hansen, R. S., *J. Catal.* **9,** 158 (1981).
16. Powell, C. J., *Surf. Sci.* **44,** 29 (1974).
17. Yates, J. T., Jr., Thiel, P. A., and Weinberg, W. H., *Surf. Sci.* **84,** 427 (1979).
18. Houston, J. E., Peebles, D. E., and Goodman, D. W., *J. Vac. Sci. Technol.* **A1,** 995 (1983).
19. Flytzani-Stephanopoulos, M., and Schmidt, L. D., *Progr. Surf. Sci.* **9,** 83 (1979).
20. Wilf, M., and Dawson, P. T., *Surf. Sci.* **60,** 561 (1976).
21. Schwaha, K., and Bechtold, E., *Surf. Sci.* **66,** 383 (1977).
22. Gland, J. L., and Kollin, E. B., *Surf. Sci.* **104,** 478 (1981).
23. Bridge, M. E., Marbrow, R. A., and Lambert, R. M., *Surf. Sci.* **57,** 415 (1976).
24. Bridge, M. E., and Lambert, R. M., *J. Catal.* **46,** 143 (1977).
25. Netzer, F. P., *Surf. Sci.* **52,** 709 (1975).
26. Conrad, H., Kuppers, J., Nitschke, F., and Netzer, F. P., *J. Catal.* **52,** 186 (1978).
27. Semancik, S., Haller, G. L., and Yates, J. T., Jr., *J. Chem. Phys.* **78,** 6970 (1983).
28. Cavanagh, R. R., and Yates, J. T., Jr., *J. Chem. Phys.* **75,** 1551 (1981).
29. Selwyn, G. S., Fujimoto, G. T., and Lin, M. C., *J. Phys. Chem.* **86,** 760 (1982).
30. Fisher, G. B., and Schmieg, S. J., *J. Vac. Sci. Technol.* **A1,** 1064 (1983).
31. Storhoff, B. N., and Lewis, H. C., Jr., *Coord. Chem. Rev.* **23,** 1 (1977).
32. Goodman, D. W., Kelley, R. D., Madey, T. E., and Yates, J. T., Jr., *J. Catal.* **63,** 226 (1980).
33. Yates, J. T., Jr., Zinck, J. J., Sheard, S., and Weinberg, W. H., *J. Chem. Phys.* **70,** 2266 (1979).
34. VanLangeveld, A. D., Van Delft, F., and Ponec, V., *Surf. Sci.* **135,** 93 (1983).
35. Winters, H. F., *J. Chem. Phys.* **64,** 3495 (1976).